A generic * shape resonance observed in energy-dependent photoelectron angular distributions from two-colour, resonant multiphoton ionization of difluorobenzene isomers

Michael Staniforth, Steven Daly, Katharine L. Reid, and Ivan Powis

Citation: The Journal of Chemical Physics **139**, 064304 (2013); doi: 10.1063/1.4817324
View online: http://dx.doi.org/10.1063/1.4817324
View Table of Contents: http://scitation.aip.org/content/aip/journal/jcp/139/6?ver=pdfcov
Published by the AIP Publishing

A generic π^* shape resonance observed in energy-dependent photoelectron angular distributions from two-colour, resonant multiphoton ionization of difluorobenzene isomers

Michael Staniforth,[a] Steven Daly,[b] Katharine L. Reid, and Ivan Powis[c]
School of Chemistry, University of Nottingham, University Park, Nottingham NG7 2RD, United Kingdom

(Received 12 June 2013; accepted 18 July 2013; published online 8 August 2013)

We present new evidence for the existence of a near threshold π^* shape resonance as a common feature in the photoionization of each isomer of difluorobenzene. Experimentally, this is revealed by significant changes in the anisotropy of the photoelectron angular distributions (PADs) following the ionization of the optically aligned S_1 state of these molecules at varying photon energies. Continuum multiple scattering Xα calculations reproduce this behaviour well, and allow the visualisation of the continuum shape resonances. The resonances are unusually narrow in energy (<1 eV), but nevertheless appear to extend right down to the ionization thresholds—exactly the low energy range typically accessed in laser-based resonance enhanced multiphoton ionization (REMPI) schemes. The anticipation of such pronounced energy dependence in the PADs and cross-sections sought for other molecules, and an ability to accurately predict such features, should be important for the reliable application and interpretation of experiments involving REMPI probing of those molecules. [http://dx.doi.org/10.1063/1.4817324]

I. INTRODUCTION

Molecular shape resonances are quite commonly encountered in both valence and core photoionization processes and arise as a consequence of the temporary trapping of the photoelectron by a potential barrier.[1–3] In such resonant trapping the amplitude of the continuum wavefunction is increased in the vicinity of the molecule, with a consequent increase, perhaps by more than an order of magnitude, in the photoionization cross-section. Because enhanced electron-nuclear coupling is anticipated at resonance,[3] vibrational branching ratios can also be influenced around the resonant energy. On the other hand, vibrational motion in the molecular target may re-distribute the resonant enhancement across a range of energy[4] so that molecular shape resonances are commonly rather broad (several eV) and the expected peaking in the total cross-section will be reduced by this spread.

Associated with a shape resonance there is also a rapid variation in the scattering phases of the resonant continuum channels. Because the photoelectron angular distribution (PAD) is an interference pattern which is highly phase sensitive, the PADs can be expected to show strong variation through a shape resonance; they therefore often provide a much more dramatic indicator of resonance than any enhancement seen in the integrated photoionization cross section alone.

Experimental study of shape resonances has been strongly facilitated in recent decades by the availability of synchrotron radiation, which offers wide ranging and convenient tunability, as well as polarization control, across those wavelength regions appropriate for the investigation of single-photon valence and core shell photoionization. However, because of the limitations of the instrumentation typically available, and perhaps because of the perception that such resonances are several eV wide, rather little attention has been focussed on the region within, say, 1 eV of the ionization threshold. Conversely, in many situations where laser multiphoton ionization (MPI) is employed this is precisely the energy regime that would be accessed. While the motivation of many MPI applications is not focussed on the photoionization dynamics per se, it is apparent that understanding the pronounced energy dependence that may be encountered in a shape resonance enhanced region will be important for an accurate interpretation of results.

In previous studies of the photoionization of the optically pumped S_1 state of *para*-difluorobenzene (*p*-DFB) we reported a very pronounced shape resonance just above the ionization threshold.[5,6] Our theoretical investigation of this resonance revealed it to be of π^* character, localised on the aromatic ring, and suggested that such a resonance may be generic to other fluorine substituted benzene compounds. In the present work we extend our experimental study to the two photon ionization of related *meta*- and *ortho*-difluorobenzene isomers (*m*-DFB, *o*-DFB, respectively) and take the opportunity to extend the previous investigation of *p*-DFB to higher electron energies using vacuum ultraviolet (VUV) laser ionization. These studies, together with accompanying

[a]Present address: Department of Chemistry, University of Warwick, Gibbet Hill, Coventry CV4 7AL, United Kingdom.
[b]Present address: Institut Lumière Matière, Université Claude Bernard Lyon, 15 rue de la Doua, 69100 Villeurbanne, France.
[c]Author to whom correspondence should be addressed. Electronic mail: ivan.powis@nottingham.ac.uk

calculations, confirm the existence of a common low energy shape resonance in this family of difluorobenzenes.

The axis labelling convention used in this paper for the three difluorobenzene isomers is as indicated,

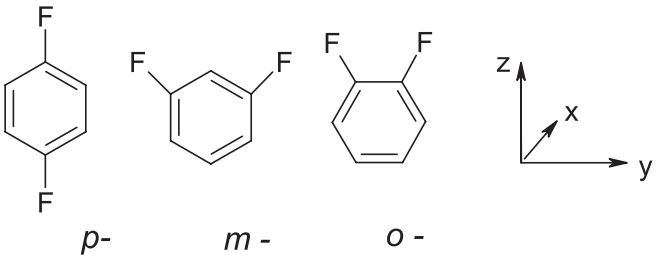

SCHEME 1.

The spectroscopy of the S_1 states of these molecules has been reported and analysed by Kable and co-workers,[7–9] while spectroscopy of the cations has been investigated by Kwon *et al.*[10] In Table I we summarise the electronic state symmetries and transitions $S_0 \rightarrow S_1 \rightarrow D_0^+ + e^-$ for the three DFB isomers and in Table II we list the S_1 vibrational levels and symmetries that have been used as intermediate states in the $(1 + 1')$ REMPI schemes employed in the present work.

II. EXPERIMENTAL

Photoelectron angular distributions were recorded using a velocity map imaging (VMI) spectrometer[11] in an arrangement that has been described previously.[12]

Pumping to the S_1 state of the target molecules (and, in some one-colour experiments, the subsequent ionization step) was accomplished with a ns Nd:YAG pumped dye laser (Continuum Surelite I : Sirah Cobra) using either Coumarin 503 or Coumarin 540a dyes whose output was doubled via a BBO crystal providing ~2 mJ/pulse in a wavelength range of 480–560 nm. For two colour work a second Nd:YAG/Dye system (Continuum Powerlite : Sirah Cobra/Stretch) was used for S_1 ionization. The output of DCM dye was tripled to provide 2–3 mJ pulses of ionizing light in the range 206–220 nm.

Alternatively, ionization was accomplished with VUV light in the range 156–174 nm. This was generated by four-wave difference frequency mixing in ~200 mbar krypton gas.[13] In this case the Kr $5p$ $[1/2]_0$ resonance was pumped by two photons at 212.494 nm from the second Nd:YAG/dye laser while a third laser system (Continuum Surelite III : ND6000) generated tunable UV light from 330 to 270 nm. The 212 nm pump beam was telescoped by two lenses with focal lengths of 20 cm and combined with the UV beam at a dichroic mirror; the merged beam was then focused into the Kr cell by a single 50 cm lens. The generated VUV was collimated with a MgF_2 lens at the exit of the gas cell and passed through a small monochromator in which a MgF_2 prism separated and directed the VUV light towards the spectrometer. A final MgF_2 lens focused the VUV light into the spectrometer. While MgF_2 has the required transmission at VUV wavelengths, it is a birefringent material, and to help preserve linear polarization from the lasers its optical axis was selected to lie perpendicular to the plane of the lenses, and vertically, along the polarisation axis, in the prism.

DFB isomer samples of 98% purity or higher (Aldrich) were seeded at room temperature in an inert gas (either helium or argon) at 2 bars pressure, and expanded through a pulsed nozzle. The resulting supersonic beam was skimmed and entered the VMI spectrometer along the instrument axis. In the VMI source region the molecular beam was then intersected by the loosely focussed laser beams, and the resulting photoelectrons were accelerated along a μ-metal shielded field-free flight region towards an imaging detector (MCP stack/phosphor screen/CCD camera). Images were accumulated over a period of an hour for two colour images, or 17 min for one colour images, at a repetition rate of 10 Hz.

TABLE I. Electronic states and transition symmetries of the difluorobenzenes.

	o-DFB (C_{2v})	*m*-DFB (C_{2v})	*p*-DFB (D_{2h})
S_0	$^1A_1$	$^1A_1$	^1A_g
HOMO → LUMO	$b_1 \rightarrow b_1$	$a_2 \rightarrow b_1$	$b_{2g} \rightarrow a_u$
S_1	$^1A_1$	$^1B_2$	$^1B_{2u}$
$S_0 \rightarrow S_1$ 0-0 polarization	z	y	y
Ion	$^2B_1$	$^2A_2$	$^2B_{2g}$
Calculated shape resonance	ka_2	kb_1	kb_{2g}
$S_1 \rightarrow k\varepsilon$ (resonant) polarization	y	z	y
$IP(S_0)$[a] (eV)	9.299	9.340	9.158
S_1 Origin 0-0 excitation (cm^{-1})	37 827[b]	37 910[c]	36 838[d]
$IP(S_1)$[e] (eV)	4.61	4.64	4.59
CMS-Xα $\Delta E_{S_1-S_0}$ (vert.) (cm^{-1})	38 421	38 640	38 524

[a]Reference 10.
[b]Reference 9.
[c]Reference 7.
[d]Reference 8.
[e]Difference $IP(S_0) - S_1$ 0-0 excitation.

TABLE II. S_1 vibrational levels used as intermediate states.

o-DFB[a]		*m*-DFB[b]		*p*-DFB[c]	
Level	Energy[d] (cm^{-1})	Level	Energy[d] (cm^{-1})	Level	Energy[d] (cm^{-1})
Origin (a_1)	0	Origin (a_1)	0	Origin (a_g)	0
20^2 (a_1)	247	11^1 (a_1)	317	6^1 (a_g)	410
30^1 (b_2)	397	9^1 (a_1)	701	5^1 (a_g)	818
9^1 (a_1)	721	8^1 (a_1)	966	5^2 (a_g)	1636
$14^1 15^1$ (a_1)	751	6^1 (a_1)	1267		
8^1 (a_1)	924	9^2 (a_1)	1402		
$14^1 18^1$ (b_2)	936				
6^1 (a_1)	1262				

[a]Reference 9.
[b]Reference 7.
[c]Reference 8.
[d]Energy relative to vibrationless origin.

A. Image analysis

For a two photon $(1 + 1')$ ionization using polarization vectors which are mutually parallel to one another and the VMI detector plane, as here, a cylindrically symmetric laboratory frame photoelectron angular distribution is expected[14]

which can be written as

$$I(\theta) = 1 + b_2 P_2(\cos\theta) + b_4 P_4(\cos\theta), \quad (1)$$

where θ is the polar angle measured from the laser polarization direction and the P_j are Legendre polynomials. The b_j are anisotropy parameters that depend on the photon-molecule dynamics.

The recorded 2D projection images were analysed using the pBasex method[15] with an angular basis of even Legendre polynomials, $l \leq 4$, to obtain the angular coefficients, b_j, and the angle integrated photoelectron spectra (PES).

In the experiments using VUV ionization a background of electrons resulting from scattered light could not be eliminated; in these cases a second background image, with molecular beam *off*, was recorded. Data treatment after subtraction of the background image was fully evaluated, but after investigation it was found preferable to analyse both images independently. The extracted PES were then subtracted to yield the background corrected (1 + 1′) PES. Similarly the recorded b_j parameters were corrected by considering them a weighted average of the true signal and any background signal. Corrected b_j parameters are then readily obtained once the background-only angular distribution has been analysed and the relative energy dependent cross-sections (PES intensities) are known.

III. THEORETICAL METHOD

As in our earlier work on *p*-DFB,[6] we treat the photoionization dynamics by a two step model that considers single photon ionization occurring from the optically prepared (and aligned) S_1 neutral. A similar approach has recently been applied to the resonance enhanced ionization of pyrazine.[16]

The general procedures we follow to compute the photoionization matrix elements using the continuum multiple scattering Xα (CMS-Xα) method have been described previously.[17] In brief, we commence by generating a self-consistent neutral molecule potential modelled from overlapping spherical regions centred on each atomic site, and all are enclosed within a spherically symmetric outer sphere that extends to infinity. Within these regions the exchange contribution to an effective one-electron potential is represented using the Xα local density approximation[18] and the wavefunctions are expressed in a symmetry-adapted basis of spherical harmonic functions on each centre, with radial functions obtained by direct numerical integration within the spherical zones of the potential.

Geometric coordinates for each molecule were taken from calculated MP2/6-31G(*p*,*d*) optimised structures in the case of the S_0 ground state, while excited neutral S_1 state geometries were found using both time-dependent density functional theory (TD-B3LYP/cc-pVTZ) or CIS/Aug-cc-pVTZ methods—all as implemented in GAUSSIAN 09 program.[19] Atomic α parameters were taken from the compilation of Schwarz[20] while radii for the overlapping atomic spheres were obtained by the Norman procedure.[21] The usual empirical scaling factor of 0.88 applied to these radii was further reduced to 0.83 for the results presented here, as discussed below. Angular basis functions on the atomic centres were truncated at either $l_{max} = 3$ (for C and F atoms) or $l_{max} = 0$ (for H atoms), while in the spherical outer region $l_{max} = 5$ was imposed; however, most calculations were repeated with these cut-off limits increased to, respectively, 5, 3, 7 to confirm acceptable convergence was achieved.

For each set of molecular parameters a trial S_0 electron density was developed by iterating to obtain a self-consistent ground state potential and the associated one-electron functions. An excited neutral S_1 potential was subsequently generated following the ansatz of promoting one electron from the relevant HOMO to the LUMO orbital,[22] maintaining these modified occupation numbers during the re-iteration to self-consistency of the S_1 potential. The estimated vertical excitation energies, $\Delta E_{S_1-S_0}$, at the S_0 equilibrium geometries are compared with experimental values in Table I.

For calculation of continuum electron functions these S_1 neutral potentials were adapted to have an asymptotic Coulombic form appropriate for ion plus electron, and the spherical harmonic basis expansions were extended to higher l_{max} [l_{max} (C,F) = 6, l_{max} (H) = 3, and l_{max} (outer sphere) = 8], reflecting the expected scattering into higher *l*-waves caused by the anisotropic ion potential. The neutral S_1 state bound orbitals were recalculated in these same modified potentials and it was also ascertained that these levels were only minimally perturbed by the asymptotic Coulombic adaptation made to the potentials. Photoionization matrix elements between the excited neutral S_1 and final (ionized) states were thus obtained in a frozen core approximation with a set of orthogonal orbital functions.

The distribution of the molecular axes in the S_1 excited state following the $S_0 \rightarrow S_1$ pump excitation can be expressed:

$$f(\chi) = 1 + a_2 P_2(\cos\chi), \quad (2)$$

where χ measures the angle of one of the molecular axes (which one depending on the pump transition moment) to the pump laser polarization. Equation (2) describes an aligned distribution of molecular axes for all nonzero values of the alignment parameter a_2. This parameter has a maximum value of 2.0, expected in the limit of short pulse excitation, but can be varied to examine depolarization of longer lived excited intermediates.

Molecule-frame photoelectron angular distributions were calculated from the photoionization matrix elements and averaged over assumed distributions of molecular orientations (Eq. (2)) to obtain predicted lab-frame photoelectron angular distributions for comparison with experiment.

Properties of the calculated continuum electron functions are conveniently visualised in a real eigenchannel representation, obtained by diagonalization of the **K**-matrix normalised functions computed by the CMS-Xα treatment.[23,24]

IV. RESULTS

Photoelectron spectra (PES) following (1+1′) REMPI were recorded by preparing each of the isomers in selected S_1 vibrational levels prior to ionization by selected probe wavelengths. Figure 1 shows a representative PES of *m*-DFB after excitation via the S_1 9^1 vibrational level and the VMI electron

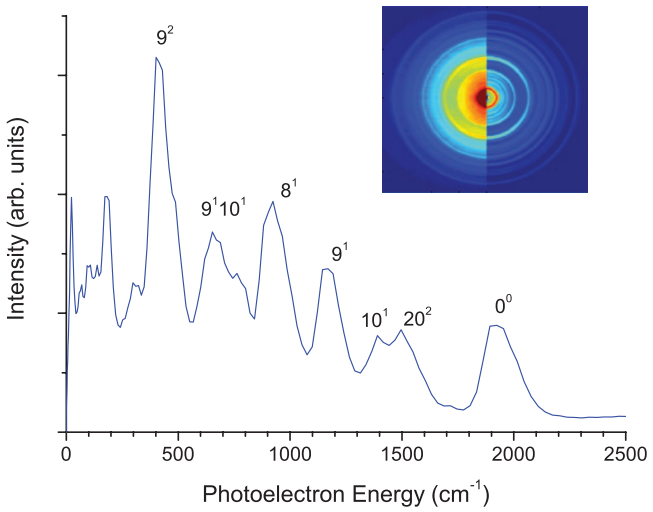

FIG. 1. (1 + 1) photoelectron spectrum (PES) of *m*-DFB recorded with 258.9 nm light (resonant at the S_1 9^1 vibrational level) with cation vibrational structure indicated following the assignments by Kwon *et al.*[10] Inset shows the VMI electron image from which the PES and angular distribution were obtained; the left half image is the raw 2D projection image, the right half image is the reconstructed 3D slice after Abel inversion.

images, from which it was derived, before and after the pBasex data treatment.

At the lower photoionization energies accessed, vibrational structure in the PES was clearly resolved, as can be seen in Fig. 1, and could be assigned by comparison with a previous mass analysed threshold ionization (MATI) study of the cation spectroscopy.[10] The associated angular parameters, b_j, could be assigned to individual vibrationally resolved transitions[25] $S_1 v^n \rightarrow D_0 v^{n+}$. At higher photoionization energies the VMI energy resolution precludes this level of separation, and so vibrational features, although still evident in the PES, can no longer be assigned to individual vibrational levels in the ion; consequently, the angular parameters associated with these observed PES peaks cannot be uniquely associated with cation vibrational states.

In Fig. 2 we compare both experimental and theoretical b_2 angular distribution parameters, as a function of photoelectron energy, for the three isomers. In the case of *p*-DFB our previously reported results[6] are also included in the figure; the new data obtained here provide additional near-threshold measurements through the preparation of the S_1 5^1 and 5^2 levels, as well as short wavelength probe experiments yielding photoelectron energies >7500 cm^{-1}. Corresponding results for the b_4 parameters are shown in Fig. 3. The error bars in both figures are generated by propagation of errors during the pBasex analysis, and are based upon an estimate of the statistical uncertainty in the raw images (assuming Poisson counting statistics); they do not explicitly include any systematic uncertainty.

The b_2 parameters for the three isomers display a striking common characteristic as a function of energy, falling rapidly through a distinct minimum, followed by a recovery back to positive values, all within ~1 eV above the ionization threshold. In our previous investigation of *p*-DFB we attributed this behaviour to a near threshold shape resonance.[6] The steepness of the initial decreases in these b_2 angular distribution parameter curves renders a visual comparison of experiment with theory very sensitive to even relatively small offsets between the experimental and theoretical energy scales. The theoretical energy scale is, however, subject to the known limitations of the Koopmans theorem approach implicit in the independent-electron CMS-Xα model. We avoid the necessity for a completely *ad hoc* re-alignment of the plotted energy scales to facilitate comparison by using an adjustment to the net attractiveness of the CMS-Xα model potentials. This can be implemented in a consistent manner for all isomers by reducing the atomic sphere radii, which is achieved by reducing the Norman scaling factor to 0.83.[21] Although this adjustment shifts the calculated resonance energy by a few tenths of an eV, it has little impact on other calculated features, such as width and depth of dips in the b_2 parameter energy dependence curves.

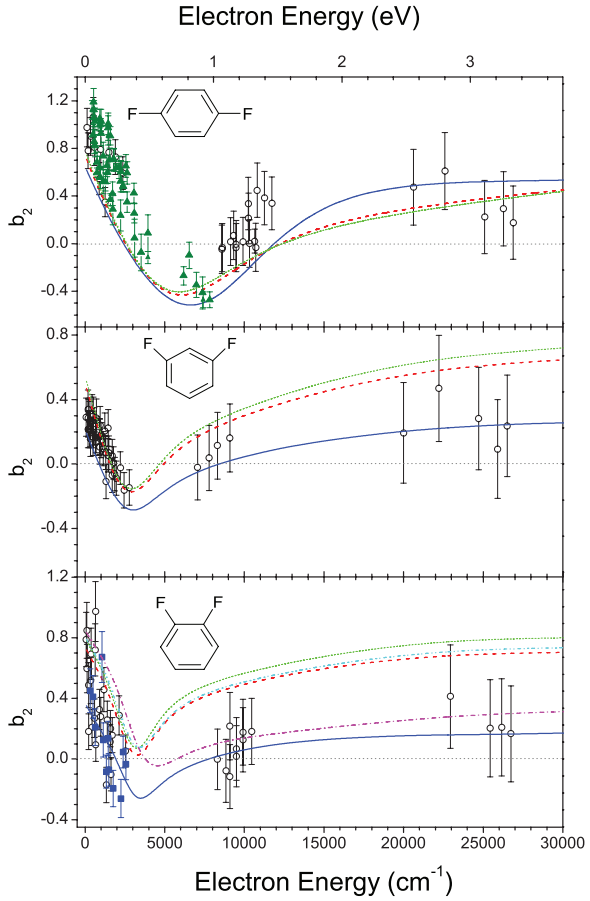

FIG. 2. Photoelectron angular distribution parameters, b_2, for *para*- (top), *meta*- (middle), and *ortho*-difluorobenzene (bottom). Experimental data: This work, ○ (black); *para*-difluorobenzene Ref. 6, ▲ (green); and *ortho*-difluorobenzene via S_1 levels of b_2 symmetry, ■ (blue). CMS-Xα calculations are also shown for differing assumed S_1 intermediate state alignment: $a_2(S_1) = 2$, solid curves (blue); $a_2(S_1) = 0.4$, dashed curves (red); and $a_2(S_1) = 0$, dotted curves (green). For *ortho*-difluorobenzene additional CMS-Xα curves indicate possible alignment following ionization via intermediate levels of b_2 symmetry for which the S_1 pump transition is *y*-polarised (see text): $a_2(S_1) = 2$, dashed-dotted curve (magenta) and $a_2(S_1) = 0.4$, dashed-dotted-dotted curve (cyan).

The nanosecond timescale of the excitation process suggests that the ionization dynamics ought to be modelled

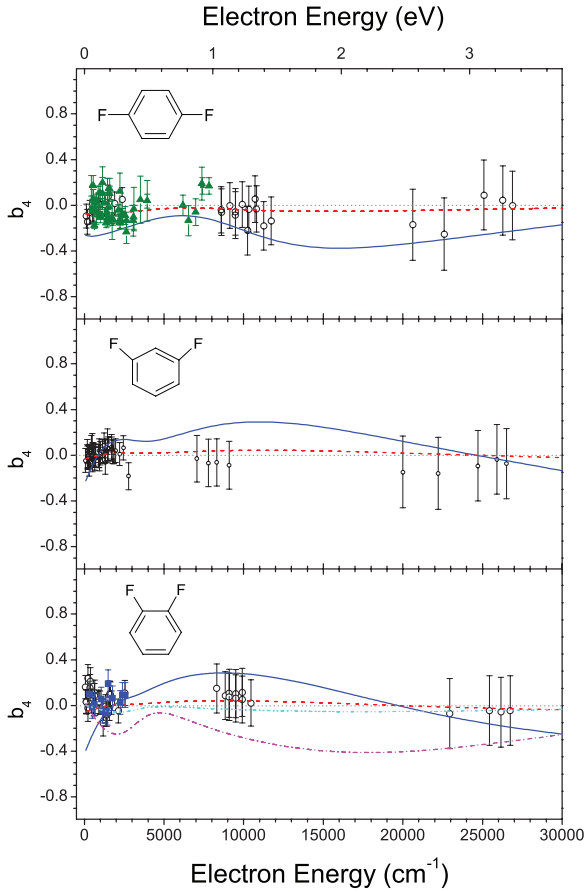

FIG. 3. Measured and calculated b_4 coefficients (see Fig. 2 for key).

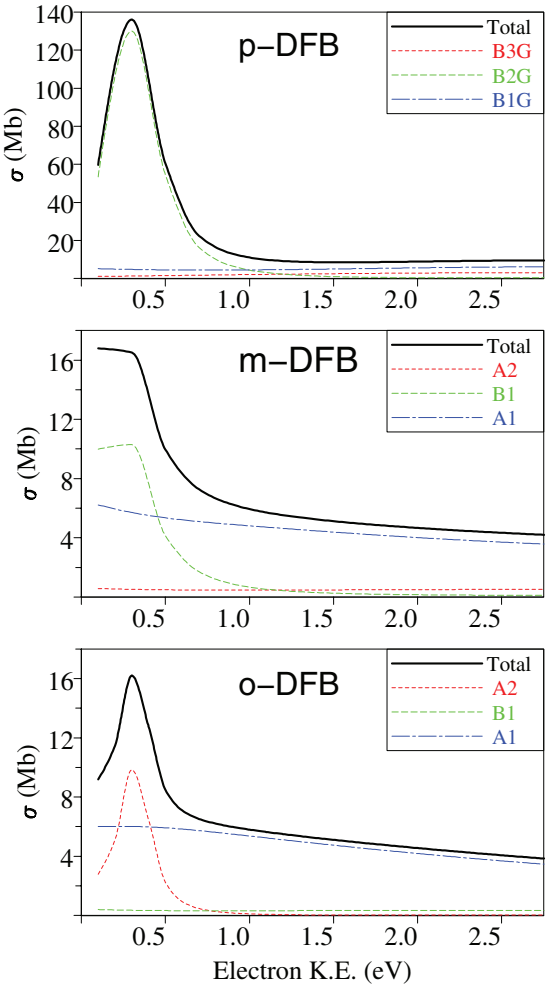

FIG. 4. Total and partial (symmetry) channel photoionization cross-sections calculated for randomly oriented S_1 states of the three difluorobenzene isomers.

from relaxed S_1 state equilibrium geometries rather than from those of the S_0 ground states. Two alternative choices for the relaxed S_1 equilibrium geometry (obtained from TD-B3LYP/cc-pVTZ or CIS/Aug-cc-pVTZ calculations) were evaluated alongside calculations performed at the fixed MP2/6-31G(p,d) S_0 geometry. For each molecule the predicted energy at which the b_2 parameter dips to a minimum changed depending on the assumed S_1 geometry. Although relatively small (∼0.3 eV), the variation in energy of the continuum features nevertheless can seem quite marked in a direct visual comparison with experiment, because of the very steep decline in b_2 values immediately above threshold, as noted above. But as also mentioned, these shifts could always be compensated by small variations in the atomic radii reduction factor so as to achieve effective agreement between calculations starting from the alternative geometry choices and with experiment. The calculations presented here are therefore based upon the MP2/6-31G(p,d) S_0 geometry, as this provides a more consistent performance across the three difluorobenzene isomers, with the same atomic radii parameter set then being applied for all three isomers.

V. DISCUSSION

A. Shape resonance

The pronounced minimum in the photoelectron energy dependence of b_2 for p-DFB has already been attributed to a low energy shape resonance.[26] It is now apparent (Fig. 2) that very similar behaviour is found for the o- and m-DFB isomers. Figure 4 shows the calculated integral total- and partial-cross-sections for photoionization of these DFB molecules, assumed to be randomly oriented in their S_1 states. For each isomer a strong enhancement of the cross-section is seen at ∼0.4 eV above threshold, which correlates with the rapid decrease in the values of the b_2 parameters already noted in the same energy region. In each isomer the resonant enhancement can be attributed to a single continuum symmetry (partial) channel, namely, $\boldsymbol{k}b_{2g}$ for p-DFB, $\boldsymbol{k}b_1$ for m-DFB, and $\boldsymbol{k}a_2$ for o-DFB. The near-threshold cross section enhancement is rather greater in p-DFB than for the other two isomers.

The continuum resonances can be further identified from examination of the eigenphase sums, $\mu_{sum} = \sum_\alpha \mu_\alpha$, which are the multichannel analogue of the single-channel central potential scattering phase shift, μ_a, encountered in formal scattering theory.[27,28] At resonance the single channel phase will show a rise of $\sim\pi$ radians, but this is often partially masked in the multichannel case by changes in the non-resonant eigenchannel phase across the same region. Figure 5 shows the eigenphase sums obtained for the $\boldsymbol{k}b_{2g}$ (p-DFB), $\boldsymbol{k}b_1$ (m-DFB), and $\boldsymbol{k}a_2$ (o-DFB) continua, and in each the very

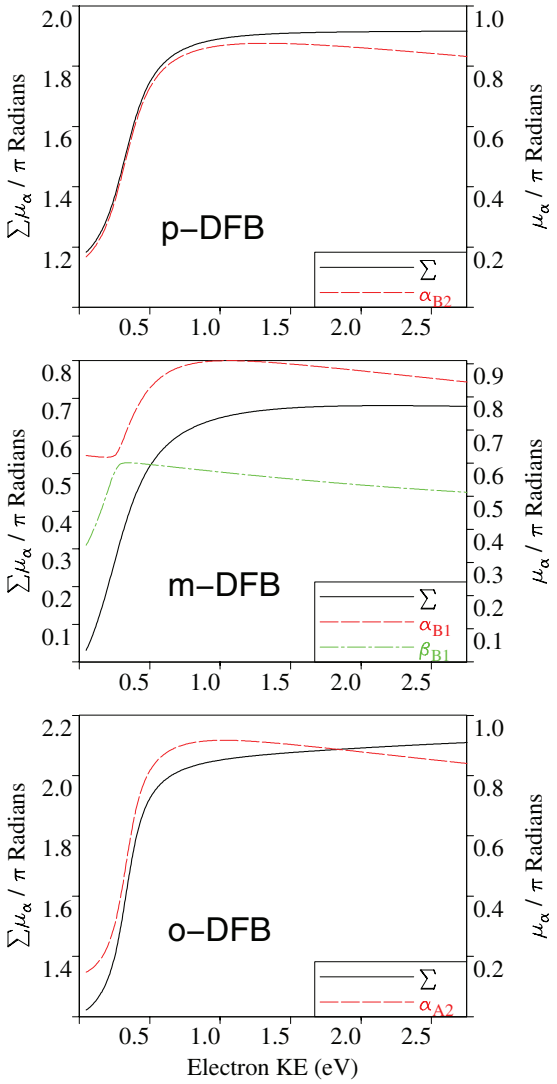

FIG. 5. Eigenphase sums, $\sum_\alpha \mu_\alpha$, for the resonant $\boldsymbol{kb_{2g}}$, $\boldsymbol{kb_1}$, and $\boldsymbol{ka_2}$ symmetry continua in, respectively, *p*-, *m*-, *o*-difluorobenzene. For each isomer the phase of the principal resonant eigenchannel(s) is also plotted. The resonances can thus be attributed to single (or for *m*-DFB, two) real eigenchannels (labelled α and, for *m*-DFB, β).

marked scattering phase rise that occurs below 0.5 eV unambiguously signifies the shape resonance in these continua. The narrow width of these resonances, indicated by the steepness of the phase increase, is unusual; molecular shape resonances are usually less pronounced and much broader.[29] It is noted that in *m*-DFB the initial rise in the eigenphase appears to be shifted below threshold, and this shift probably accounts for the slightly different shape of the predicted cross section curve at threshold (Fig. 4).

Further characterisation of the continuum can be developed following diagonalization of the K-matrix normalised CMS-Xα functions to obtain individual, real eigenchannels.[23] From examination of the individual eigenchannel phases, μ_a, we find that the resonance is carried by a single eigenchannel in *p*-DFB and *o*-DFB, and just two eigenchannels in *m*-DFB. These individual resonant eigenchannel phases are also included in Fig. 5 where it is clearly seen that they must constitute the dominant terms in the overall eigenphase sums.

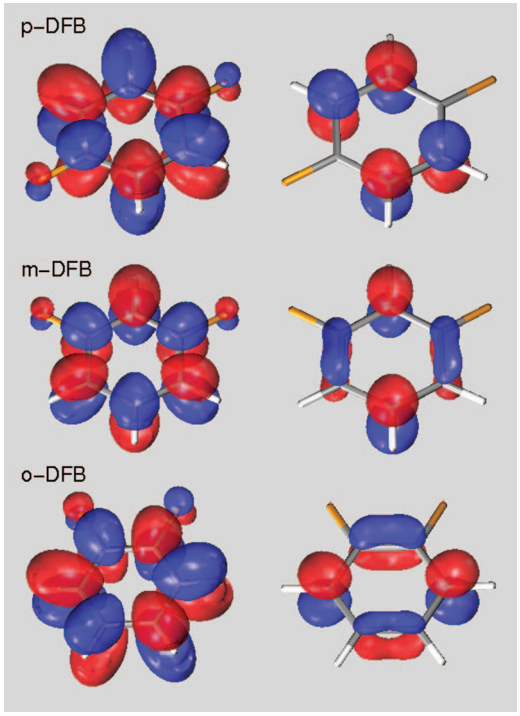

FIG. 6. Iso-surface representations of: the resonant eigenchannels α in the three isomers at a common energy 0.35 eV above the respective threshold (left column); the S_0 LUMO orbitals from a minimal basis Hartree-Fock calculation (right column).

The avoided crossings in the *m*-DFB $\boldsymbol{kb_1}$ resonant eigenphase curves indicate a strong mixing of the eigenchannels at the shape resonance[28] and the characteristics of these mutually resonant *m*-DFB eigenchannels are found to be quite similar.

The eigenchannel analysis also allows visualisation of the resonance by enabling the real eigenchannel functions to be plotted. In Fig. 6 we provide 3D iso-surface representations of the resonant eigenchannels at a common resonance energy of 0.35 eV. The common π^* character of the resonant state in each of the isomers is immediately apparent, and all three are similar to the Hartree Fock $3b_{2g}$ virtual π^* orbital in benzene, albeit with some additional π density on the F atoms. If one then focuses on the common ring-based feature of these continuum resonant states, a characteristic angular momentum, $l = 4$, can clearly be identified from the four angular nodes: three bisecting nodal planes perpendicular to the ring and one nodal plane coinciding with the ring. A classic view of shape resonances attributes them to the trapping associated with the centrifugal barriers for outgoing waves of such relatively large angular momentum.[1]

A single photon ionization of the HOMO (b_{2g}) orbital of *p*-DFB to the $\boldsymbol{kb_{2g}}$ continuum is parity forbidden, as would be an analogous ionization in benzene, so that the shape resonance seen here is only accessible in the two photon excitation. For *m*- and *o*-PDFB the corresponding $\boldsymbol{kb_1}$ and $\boldsymbol{ka_2}$ are symmetry allowed in a direct one-photon ionization from S_o as well as in the two photon ionization via S_1 studied here. Nevertheless, it may be noted that unlike the respective HOMO π orbitals, the LUMO π orbitals (shown in Fig. 6), which are those ionized from the S_1 states are, like the shape resonant states, localised on the ring, but with a clear $l = 3$

character (only two bisecting nodal planes perpendicular to the ring). Thus an anticipated $\Delta l = +1$ propensity rule for the ionization suggests the S_1 photoionization to the corresponding shape resonance seen here may be particularly prominent. A similar argument, but conversely favouring access to a near threshold shape resonance by single photon ionization was recently explored in a study of 2-butyne photoionization.[30]

The above discussion prompts the question whether a similar shape resonance may be found in other, halogen substituted benzenes. In C_6F_6, as in benzene itself, a low lying π^* resonance as here will be symmetry forbidden in single photon ionization, although a higher lying σ resonance with almost antithetical properties has been studied.[31] Both 1,3,5-trifluorobenzene (D_{3h}) and mono fluorobenzene (C_{2v}) possess similar $l = 4\,\pi^*$ virtual orbitals (respectively, a_2'' and b_1 symmetry) which could be expected to correlate with symmetry allowed shape resonant scattering states. Preliminary CMS-Xα calculations indicate that this is the case for trifluorobenzene, with a predicted resonance energy shifted up to ~3.5 eV, but for fluorobenzene the indications appear to suggest that the resonance position is shifted to just below threshold.

B. Effect of S_1 intermediate state alignment

The theoretical results that are presented in Figs. 2 and 3 treat three limiting scenarios that describe possible alignment of the intermediate S_1 state immediately prior to ionization by a probe photon: (1) full alignment ($a_2 = 2$) of the $S_0 \rightarrow S_1$ transition dipole moment (expected to lie along y for *p*-DFB and *m*-DFB and along z for *o*-DFB) about the pump polarization axis; (2) reduced alignment ($a_2 = 0.4$) corresponding to the long-time limit[32] where molecular rotations have become dephased (i.e., allowing for a lifetime of the intermediate S_1 state prior to its ionization that clearly exceeds the characteristic rotational period); (3) no alignment ($a_2 = 0.0$, and consequently $b_4 = 0$). This last case would be appropriate when collisional reorientation of the rotational axes destroys any optical pumped alignment of the S_1 state, resulting in a fully randomised molecular orientation (as is already assumed for the S_0 ground state sample) prior to ionization. In practice, such collisions can be discounted given the pressure/timescales applying to these experiments but this case provides a reference to help judge the sensitivity displayed to alignment of the molecular axes in the S_1 state.

In the case of the *p*-DFB b_2 results (Fig. 2) the assumed S_1 alignment has a relatively small effect, and the theory-experiment comparison could not be said to favour any particular assumption. The calculated b_2 parameters for *m*-DFB and *o*-DFB isomers on the other hand display a greater alignment sensitivity, and comparison with experiment (Fig. 2) now appears to favour the suggestion of a near maximal alignment ($a_2 \approx 2.0$) in these isomers.

It was previously estimated in experiments using ns laser pulses,[6] under similar conditions to the present study, that the ionizing laser flux was sufficient for the mean lifetime of S_1 *p*-DFB prior to ionization to be as short as ~10 ps; much shorter than the anticipated rotational period of the molecules in the cooled molecular beam. This deduced short lifetime was seemingly corroborated by the experimental invariance of the angular distribution when ps laser pulses were instead used. Apart from effects attributable to the multi-mode ns laser beam characteristics, the inferred short S_1 lifetime stemmed also from the large predicted photoionization cross-section, making ionization quite facile. Applying the same reasoning to the *m*- and *o*-DFB isomers for which, as seen in Fig. 4, the expected resonant enhancement of photoionization cross sections is nearly an order of magnitude less, leads to estimated lifetimes of ~100 ps. This would still fall short of the expected long-lived alignment limit ($a_2 \approx 0.4$) in these jet-cooled molecules, so we can anticipate a degree of intermediate alignment characterized by $a_2 > 0.4$ for all three molecules in these experiments.

A number of data points for *o*-DFB were obtained after preparing S_1 vibrational levels of b_2 symmetry (Table II). The $a_1 \otimes b_2$ vibronic symmetry dictates that the transition dipole moment on excitation lies parallel to the *y* axis, i.e., perpendicular to its orientation in the cases considered above. In order to model this situation an additional set of CMS-Xα curves ($a_2 = 2.0, 0.4$) have been included in Fig. 2; these suggest that the b_2 angular distribution parameter shifts to more positive values with such alignment. However, it is difficult to discern any alternative trends in the relevant experimental data below 3000 cm^{-1}, and the error bars obtained do not allow success or failure of this alternative alignment assumption to be judged.

Corresponding results for the b_4 parameters calculated with different degrees of assumed alignment are shown in Fig. 3. In principle b_4 can range from -1 to $2\frac{1}{3}$ (actual limits depending on the accompanying b_2 parameter), but to within the indicated uncertainty (Fig. 3) our experimental values scarcely differ from zero. This is consistent with the calculated values of b_4 that are included in Fig. 3 which also remain close to zero, even for assumed strong intermediate alignments. Since the b_4 parameters are necessarily zero when the ionizing photons are absorbed by a fully randomly oriented distribution (i.e., in the absence of intermediate state alignment) one might intuitively have expected the converse—that b_4 would have a significant magnitude because of the degree of intermediate state alignment that has been inferred. Evidently this is not the case here. We note, however, that in certain other investigations of (1 + 1) resonantly ionized PADs, b_4 parameters having a significant non-zero magnitude have been found—for example, $-0.09 \geq b_4 \geq -0.45$ for acetylene ionized via its aligned A state.[33] In practice, then, the alignment sensitivity reflected in b_4 appears to depend subtly on specific detail of the photoionization dynamics. It is further interesting to note that here, for these difluorobenzene systems, the b_4 parameter appears significantly less sensitive than does the b_2 parameter to the shape resonance.

C. Vibrational dependence

For the *o*-DFB results in particular, many of the experimental data points have been fully assigned to initial S_1 vibrational level (see Table II) *and* final cation vibrational level.[10,25] An effort was made to discern any simple, systematic variation of the experimental observations with as-

signed vibrational levels, but none was found. This same conclusion was reached in our previous investigation of pDFB.[6]

The exceptionally narrow nature (<1 eV) of the near threshold π^* shape resonance observed in these molecules itself argues against a strong vibrational dependence. It has been demonstrated, for example, in studies of diatomic molecules,[4] that the exact energy of a shape resonance can be strongly correlated with nuclear geometry, and consequently vibrational motion can effectively smear out the resonant enhancement, broadening the inherent width of the resonance by several eV. This can be understood as a tuning of the de Broglie wavelength required for constructive interference of a backscattered wave from an adjacent nucleus. The atypically weak electron-nuclear coupling which is inferred in the present case can, however, be ascribed to the clear π^* character of the resonance, which has displaced electron density from the internuclear regions to sit above and below the molecular plane, reducing the dependence on a simple model of internuclear backscattering.

Nevertheless, we can recall that the calculated resonance positions do vary with the chosen fixed molecular geometry (S_0 MP2/6-31G(*p*,*d*), S_1 TD-B3LYP/cc-pVTZ, S_1 CIS/aug-cc-pVTZ), when all else is maintained equal in the CMS-Xα calculation, to the extent of ~0.3 eV. This may then imply that some of the apparent scatter in the experimental b_2 data for all three isomers in the resonant region below 0.5 eV, where generally the data are fully vibrationally resolvable, is indeed attributable to a weakly enhanced electron-nuclear coupling at resonance. The failure to detect any simple *systematic* pattern of vibrational dependence does not preclude this possibility, as in a complex multidimensional system the projection of initial and final vibrational wavefunctions and coupling with geometry-dependent electronic matrix elements could well be expected to be complex and soluble only through a putative full numerical calculation.

VI. CONCLUSIONS

These results clearly demonstrate the presence of an intense, narrow π^* shape resonance in the photoionization of the three difluorobenzene isomers which sits immediately above the ionization threshold. For each isomer the resonance causes very rapid variations in the observed b_2 angular distribution parameters (equivalent to the β parameter for randomly oriented target species) which switch from positive to negative values within an energy range of just few tenths of an eV. This effect is greatest for *p*-DFB, amounting to a swing from half the expected maximal (+2) to half the minimal (−1) β parameter within 1 eV of threshold. Extending our earlier observations, we argue that the significance of a single measured PAD can only be understood if the resonant behaviour of the molecule in question is known.

Despite the different symmetry labels (occasioned by a different molecular point group for *p*-DFB, and different orientation of the principal axis through the molecular plane in the *m*- and *o*-DFB isomers) the resonance is clearly generic to these molecules and can be associated with the virtual antibonding π orbital in the parent benzene ring of each molecule.

A good agreement with experimental b_2 angular distribution parameters is established by the theoretical calculations presented here, as long as alignment of the intermediate S_1 state is fully allowed for. Particularly in the cases of *m*- and *o*-DFB, any assumption of a long-lived S_1 state alignment limit generates significantly worse agreement with experiment. This, in a sense, complements an earlier finding for *p*-DFB that the use of either ns or ps laser pulses produced little significant change in the observed PADs. Hence, the evidence and its interpretation offered here are consistent with a short ps lifetime of the prepared S_1 states of these molecules prior to their subsequent ionization, despite the ns laser pulses used in the experiments.

ACKNOWLEDGMENTS

We acknowledge EPSRC Grant No. EP/C50013X. Computing resources for calculating optimised geometries were provided by the NSCCS (EPSRC).

[1] J. L. Dehmer, D. Dill, and A. C. Parr, in *Photophysics and Photochemistry in the Vacuum Ultraviolet*, edited by S. P. McGlynn, G. L. Findley, and R. H. Huebner (D. Reidel, Dordrecht, 1985), p. 341.
[2] V. McKoy, T. A. Carlson, and R. R. Lucchese, J. Phys. Chem. **88**, 3188 (1984); M. N. Piancastelli, J. Electron Spectrosc. Relat. Phenom. **100**, 167 (1999).
[3] E. D. Poliakoff and R. R. Lucchese, Phys. Scr. **74**, C71 (2006).
[4] J. L. Dehmer, D. Dill, and S. Wallace, Phys. Rev. Lett. **43**, 1005 (1979).
[5] S. M. Bellm, P. T. Whiteside, and K. L. Reid, J. Phys. Chem. A **107**, 7373 (2003).
[6] S. M. Bellm, J. A. Davies, P. T. Whiteside, J. Guo, I. Powis, and K. L. Reid, J. Chem. Phys. **122**, 224306 (2005).
[7] P. A. Graham and S. H. Kable, J. Chem. Phys. **103**, 6426 (1995).
[8] A. E. W. Knight and S. H. Kable, J. Chem. Phys. **89**, 7139 (1988).
[9] A. K. Swinn and S. H. Kable, J. Mol. Spectrosc. **191**, 49 (1998).
[10] C. H. Kwon, H. L. Kim, and M. S. Kim, J. Chem. Phys. **118**, 6327 (2003).
[11] A. T. J. B. Eppink and D. H. Parker, Rev. Sci. Instrum. **68**, 3477 (1997).
[12] S. M. Bellm and K. L. Reid, Chem. Phys. Lett. **395**, 253 (2004).
[13] J. P. Marangos, N. Shen, H. Ma, M. H. R. Hutchinson, and J. P. Connerade, J. Opt. Soc. B **7**, 1254 (1990).
[14] K. L. Reid, Ann. Rev. Phys. Chem. **54**, 397 (2003).
[15] G. A. Garcia, L. Nahon, and I. Powis, Rev. Sci. Instrum. **75**, 4989 (2004).
[16] Y. I. Suzuki and T. Suzuki, J. Chem. Phys. **137**, 194314 (2012).
[17] Y. Hikosaka, J. H. D. Eland, T. M. Watson, and I. Powis, J. Chem. Phys. **115**, 4593 (2001); P. Downie and I. Powis, *ibid.* **111**, 4535 (1999).
[18] J. C. Slater, *The Self-Consistent Field for Molecules and Solids* (Mc-Graw Hill, New York, 1974).
[19] M. J. Frisch, G. W. Trucks, H. B. Schlegel *et al.*, GAUSSIAN 09, Revision A.02, Gaussian Inc., Wallingford, CT, 2009.
[20] K. Schwarz, Phys. Rev. B **5**, 2466 (1972).
[21] J. G. Norman, J. Chem. Phys. **61**, 4630 (1974).
[22] O. Gunnarsson and B. I. Lundqvist, Phys. Rev. B **13**, 4274 (1976).
[23] D. Loomba, S. Wallace, D. Dill, and J. L. Dehmer, J. Chem. Phys. **75**, 4546 (1981).
[24] I. Powis, J. Chem. Phys. **106**, 5013 (1997).
[25] M. Staniforth, Ph.D. thesis, University of Nottingham, 2011.
[26] S. M. Bellm and K. L. Reid, Phys. Rev. Lett. **91**, 263002 (2003).
[27] A. U. Hazi, Phys. Rev. A **19**, 920 (1979).
[28] J. Macek, Phys. Rev. A **2**, 1101 (1970).
[29] W. Thiel, J. Electron. Spectrosc. Relat. Phenom. **31**, 151 (1983).
[30] H. Xu, U. Jacovella, B. Ruscic, S. T. Pratt, and R. R. Lucchese, J. Chem. Phys. **136**, 154303 (2012).
[31] A. Das, E. D. Poliakoff, R. R. Lucchese, and J. D. Bozek, J. Chem. Phys. **125**, 164316 (2006).
[32] R. N. Zare, Ber. Bunsenges. Phys. Chem. **86**, 422 (1982); E. H. van Kleef and I. Powis, Mol. Phys. **96**, 757 (1999).
[33] P. Hockett, A. K. King, I. Powis, and K. L. Reid, J. Chem. Phys. **127**, 154307 (2007).